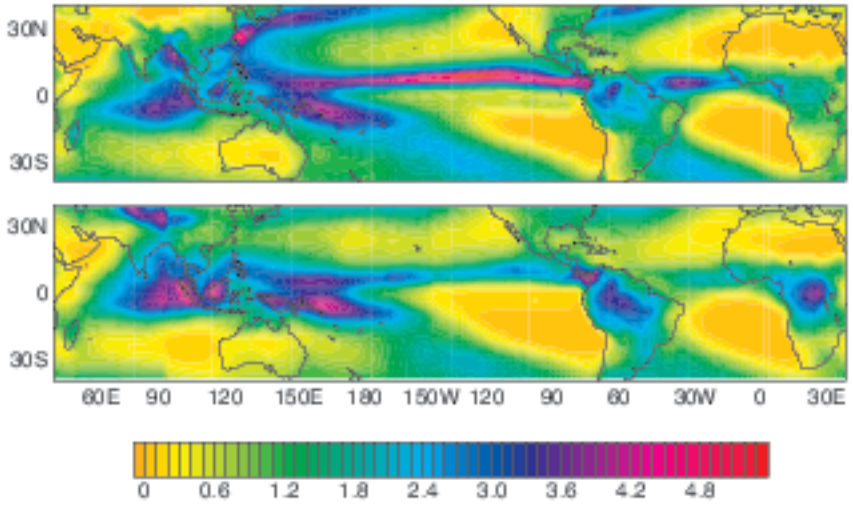

Figure 1. Annual mean precipitation over the tropics, as inferred from different data sources. The upper panel is based on the microwave sounding unit over the ocean and a land climatology compiled from station data. The lower panel shows the Geostationary Operational Environmental Satellite precipitation index (GPI) inferred from high-resolution imagery of outgoing longwave radiation. The bands of heavy precipitation over the tropical Pacific and Atlantic are the oceanic ITCZs. Quantitative estimates of precipitation in meters per year can be inferred from the color bar at the bottom.

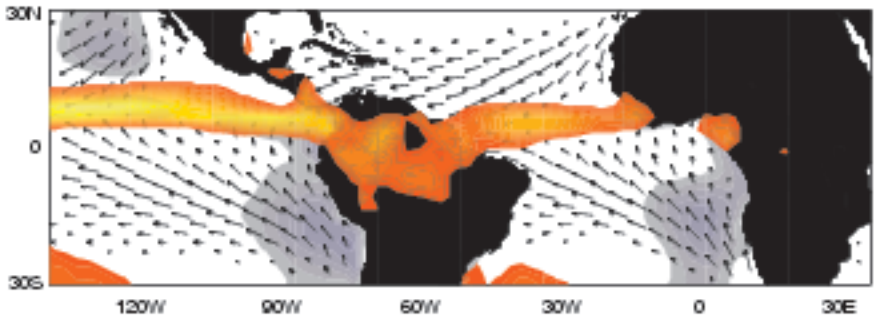

Figure 2. Climatological annual mean conditions over the Pan American region. Vectors denote surface winds, orange-yellow shading denotes precipitation, and gray-blue shading denotes stratus cloud decks. Over both the Atlantic and Pacific, the ITCZ is located well to the north of the equator, and southeasterly trades extend across the equator. The stratus cloud decks are more extensive in the Southern Hemisphere.

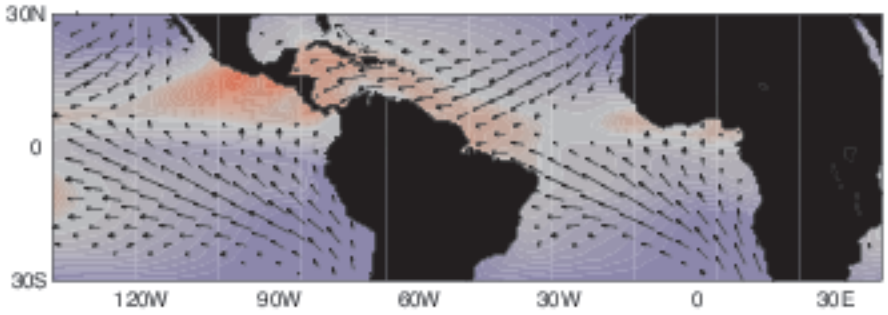

Figure 3. As in Fig. 2, but shading denotes annual mean sea surface temperature. The warmest (reddest) waters are observed, not on the equator, but in the Northern Hemisphere near the latitude of the ITCZ.

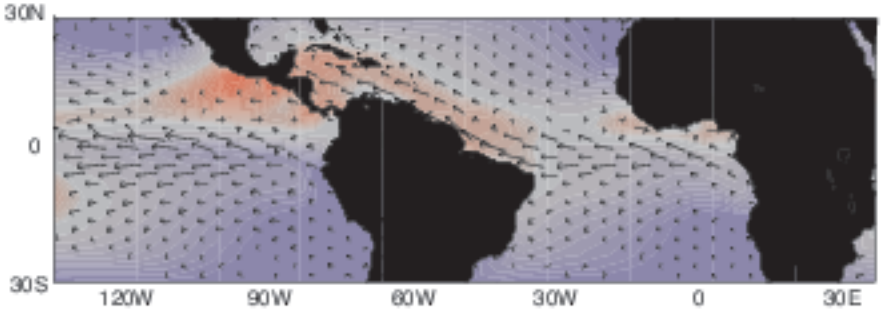

Figure 4. As in Fig. 3, but arrows denote surface currents. The eastward arrows at the latitude of the ITCZ correspond to the North Equatorial Countercurrent and the longer westward arrows along and just to the south of the equator correspond to the South Equatorial Current.

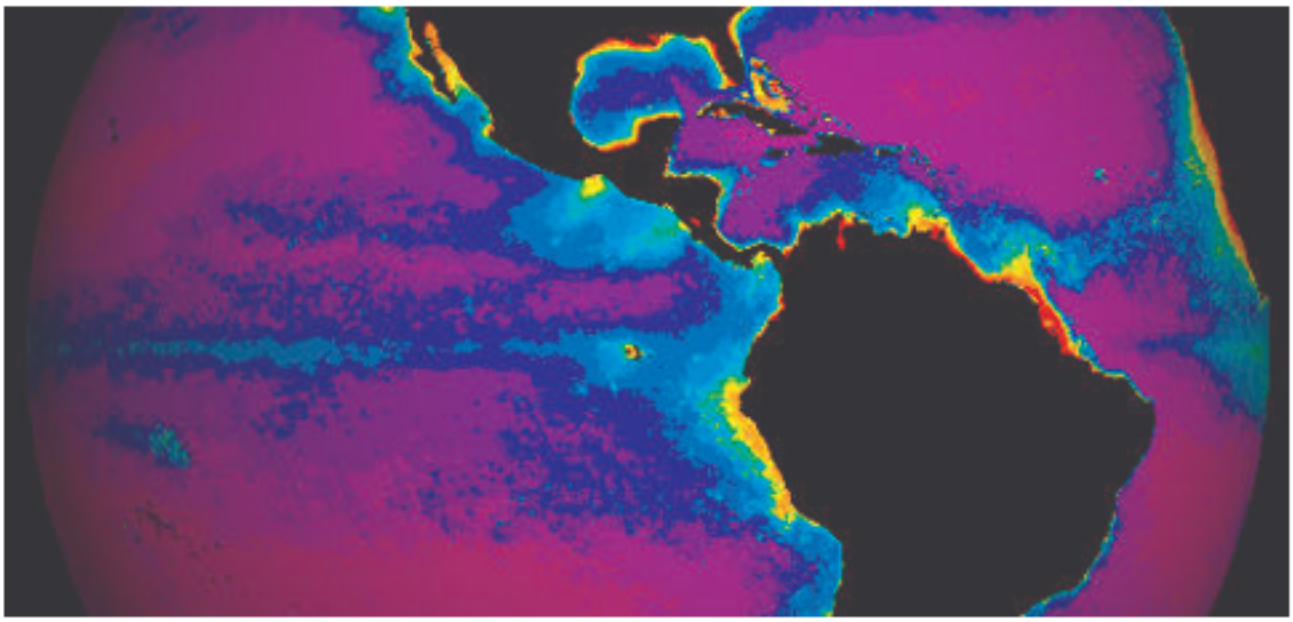

Figure 5. Annual mean chlorophyll concentrations based on Coastal Zone Color Scanner imagery. The color scale has been adjusted to enhance the weak gradients in the vicinity of the equator. The enhanced concentrations along the equator in both oceans are signatures of upwelling. Concentrations are also enhanced beneath the ITCZ, in the region of coastal upwelling along the Peruvian coast and downstream (on the Pacific side) of the gaps in the mountain ranges of Central America.

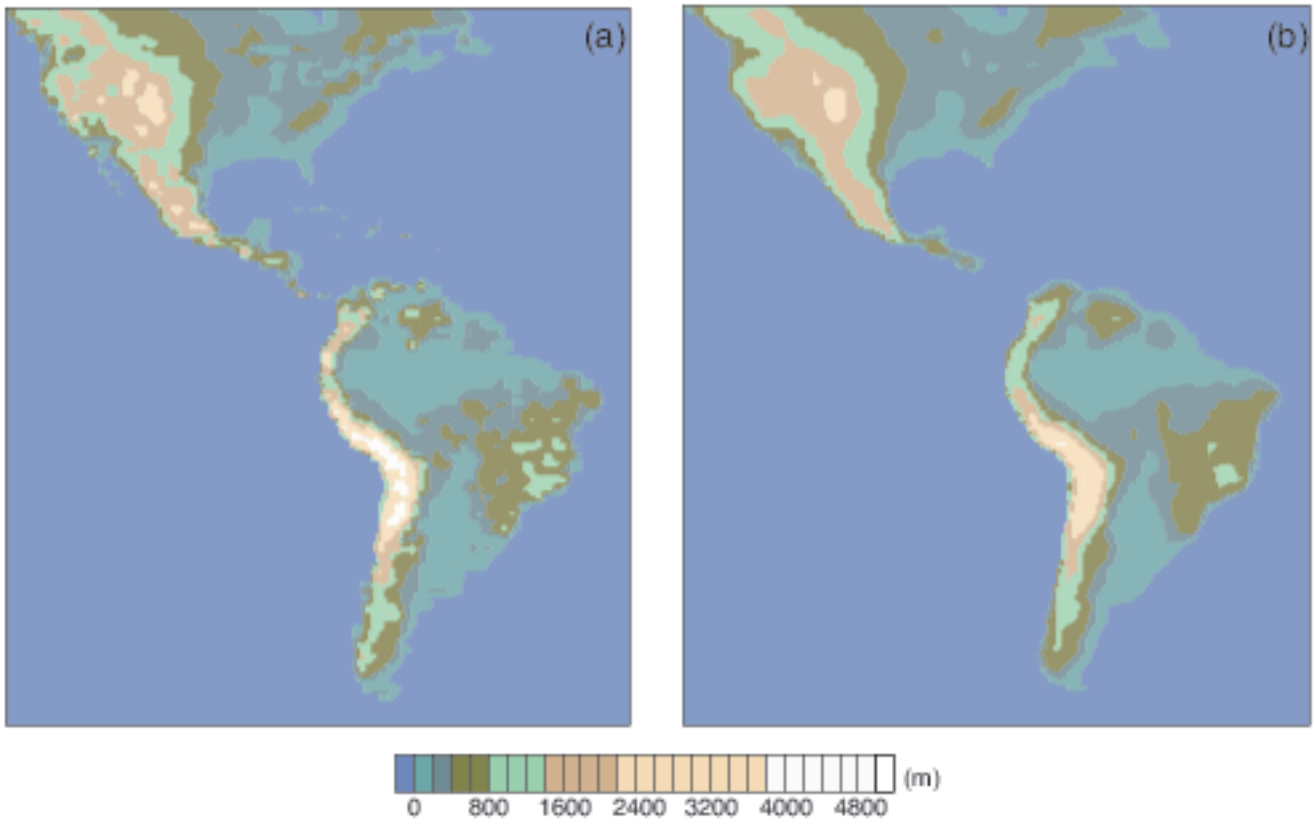

Figure 6. Topography of North and South America, (a) at approximately 5' resolution and (b) at the typical 2° latitude-longitude resolution of an atmospheric general circulation model that is used in climate simulations. Shading interval is 200 m.

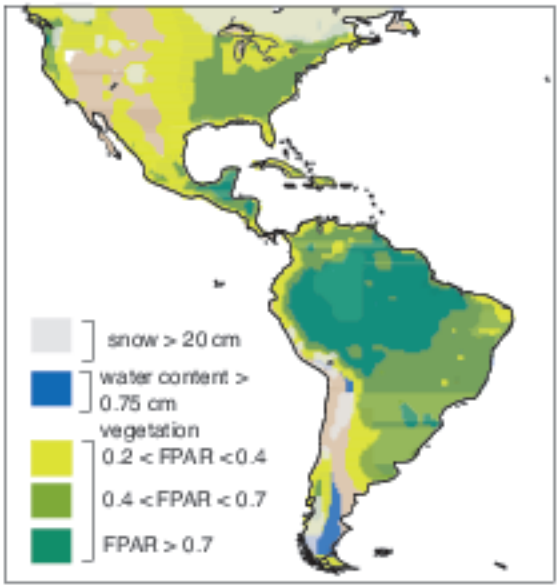

Figure 7. Annual mean distribution of snow, soil moisture, and vegetation over North and South America. The soil moisture is characterized by model water content in the topmost 7 cm of soil. Vegetation is documented by the satellite-derived fraction of photo-synthetically active radiation absorbed by the green vegetation canopy (FPAR). Snow depth derived from surface observations.

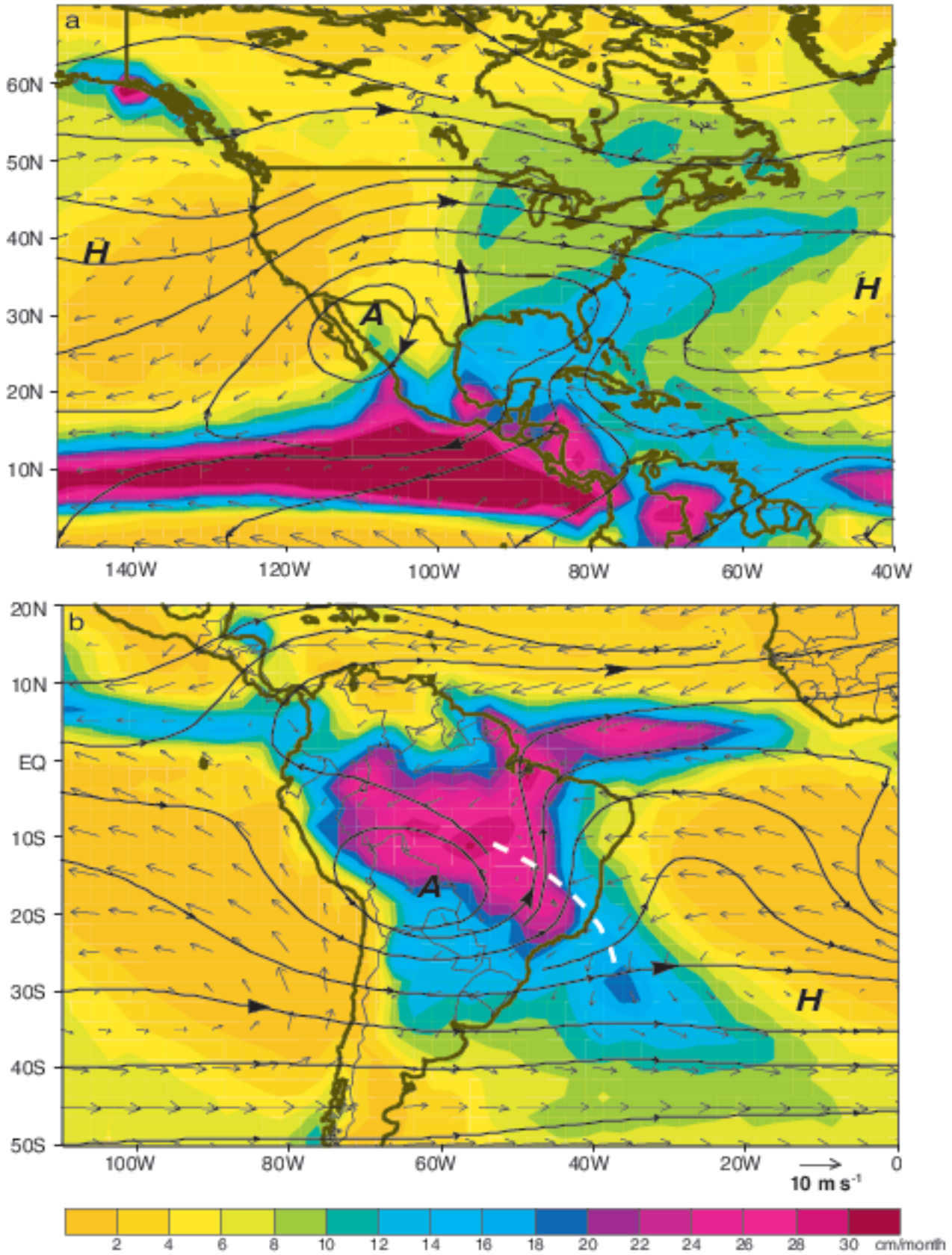

Figure 8. Mean (1979-1995) warm season precipitation (shading) and circulation at 925 hPa (vector winds) and 200 hPa (streamlines): a) July-September. The position of upper-level monsoon anticyclone over the southwestern United States and northwestern Mexico is indicated by an "A". The subtropical surface high pressure centers over Bermuda and the North Pacific are indicated by "H". The approximate location of the Great Plains low-level jet is indicated by a heavy solid arrow. b) December-February. The position of the upper-level monsoon high over Bolivia is indicated by an "A". The South Atlantic subtropical surface high pressure center is indicated by an "H". The approximate axis of the South Atlantic Convergence Zone (SACZ) is indicated by the heavy white dashed line.

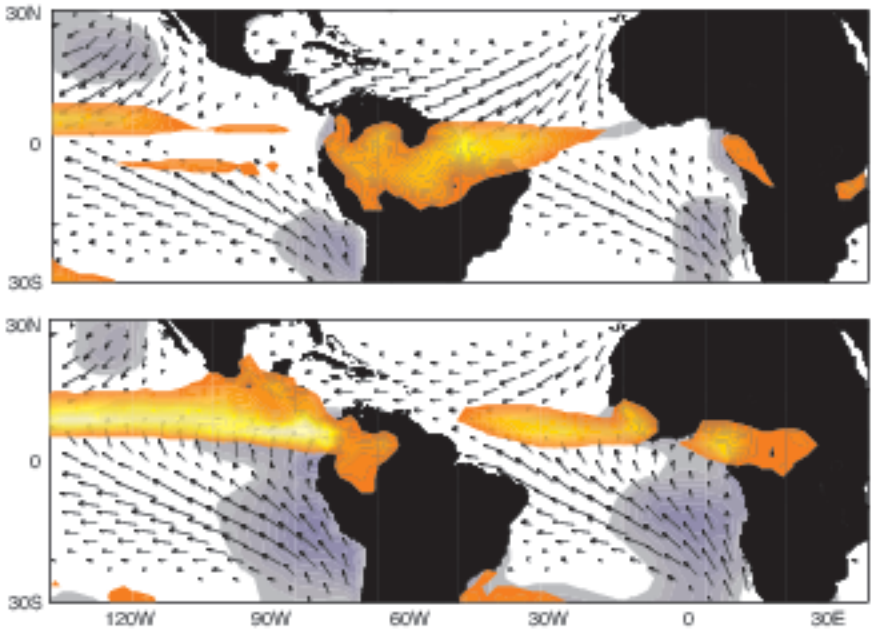

Figure 9. As in Fig. 2, but for the March-April mean (upper panel and September-October mean conditions (lower panel). Note the double ITCZ configuration in the Pacific, symmetric about the equator in March-April, in contrast to the prominent single ITCZ near 10°N in September. A strongly contrasting structure is also observed in the Atlantic sector, with the ITCZ displaced farther north in September-October. Rainfall rates in excess of 20 cm per month are colored orange-yellow.

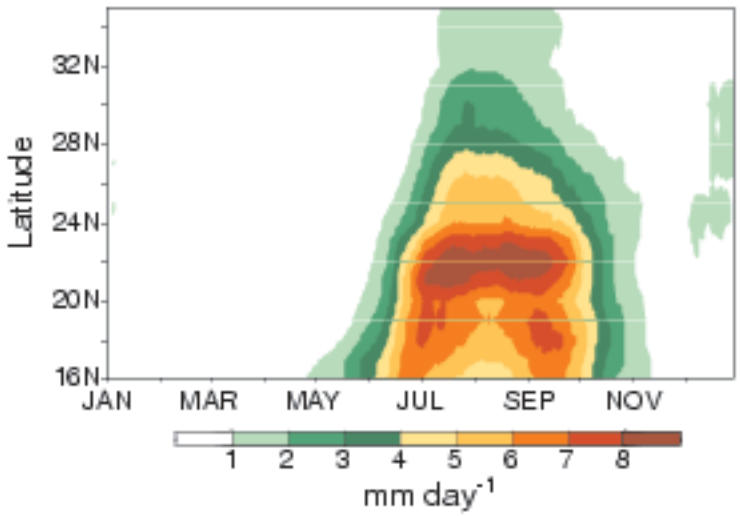

Figure 10. Time-latitude sections of the mean (1961-1990) annual cycle of precipitation. Data are averaged zonally over west coast land points at each latitude.

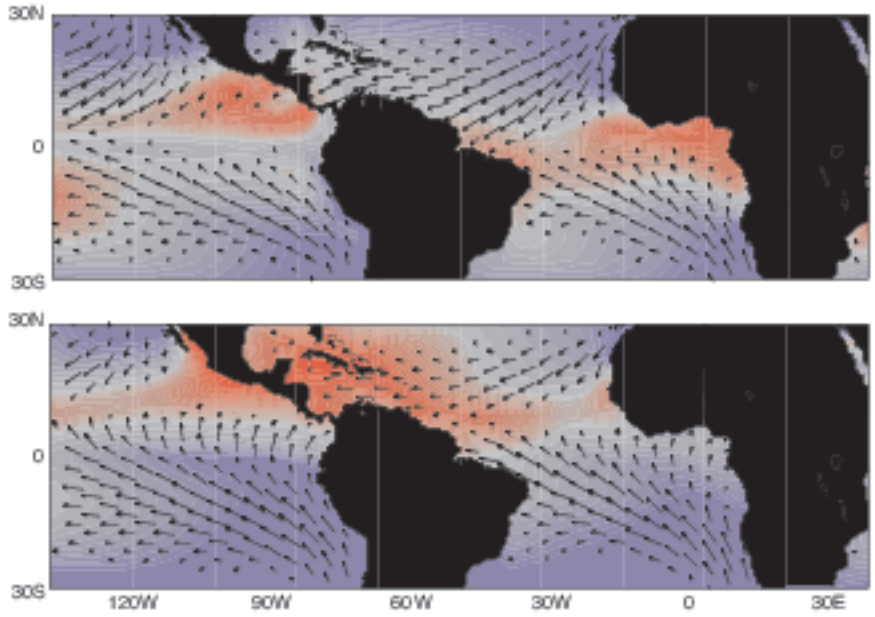

Figure 11. As in Fig. 3 but for the March-April mean (upper panel) and September-October mean conditions (lower panel). The warm pool to the north of the equator is present year round. The largest seasonal contrasts are observed along the southern flank of the equatorial cold tongue. September-October is the time of strongest meridional temperature contrast across the equator.

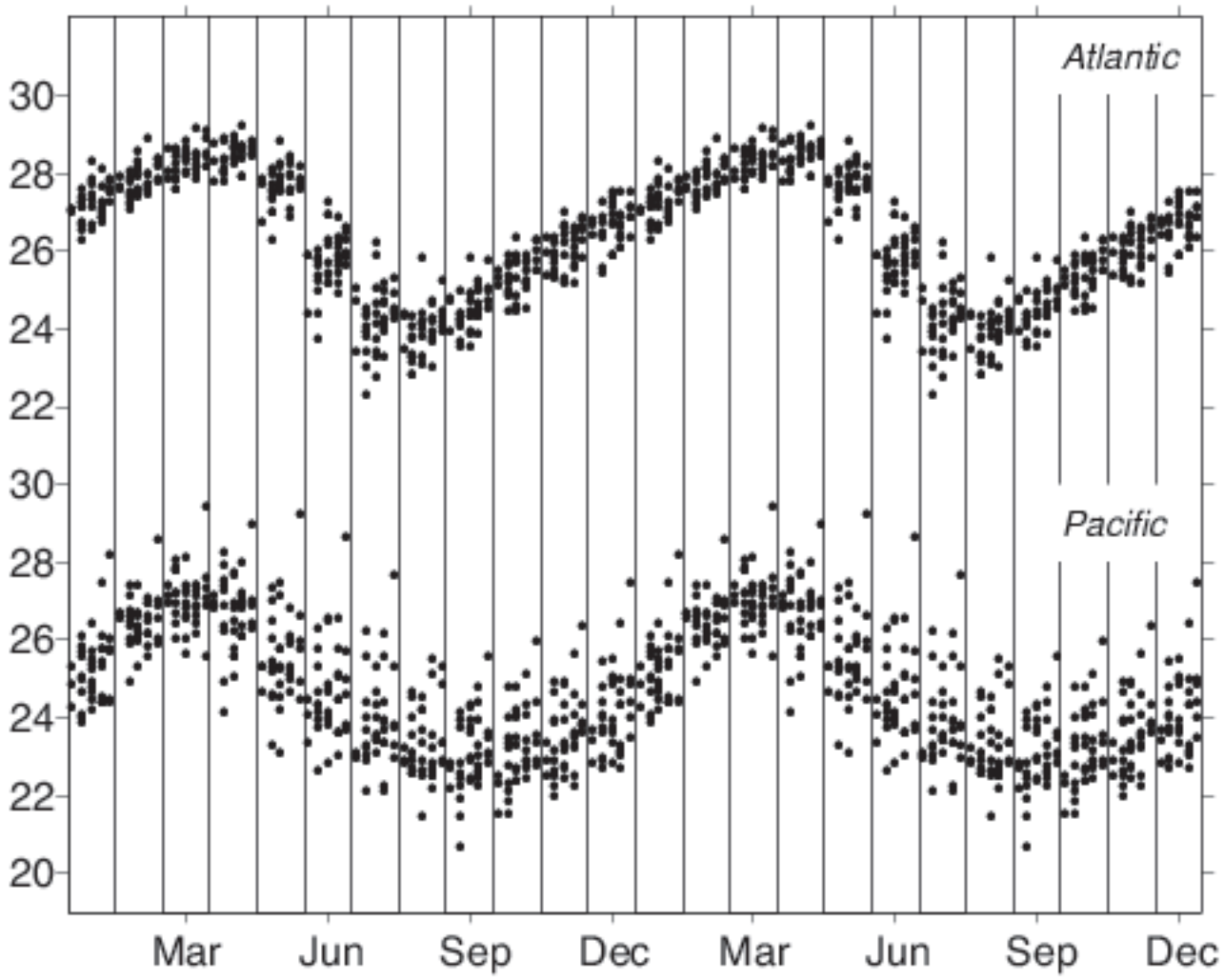

Figure 12. Scatter plot of monthly mean sea surface temperature (°C) in the equatorial cold tongue regions of the Atlantic and Pacific for individual years/months, grouped by calendar month. The dots for each calendar month are staggered along the *x* axis to make them more visible, and the calendar year is repeated. Note the high degree of reproducibility of the seasonal march, particularly in the Atlantic, where El Niño exerts only a modest influence.

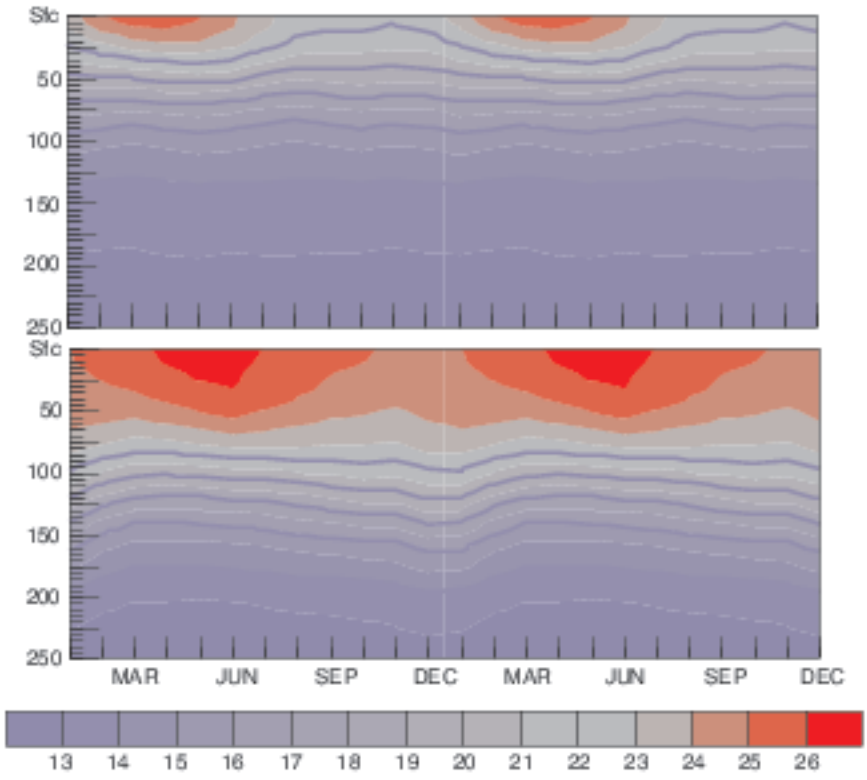

Figure 13. Depth-time sections of climatological mean temperature (°C) on the equator at 110°W (upper panel) and 140°W (lower panel) showing how the seasonal march tends to be much stronger near the surface than near the thermocline.

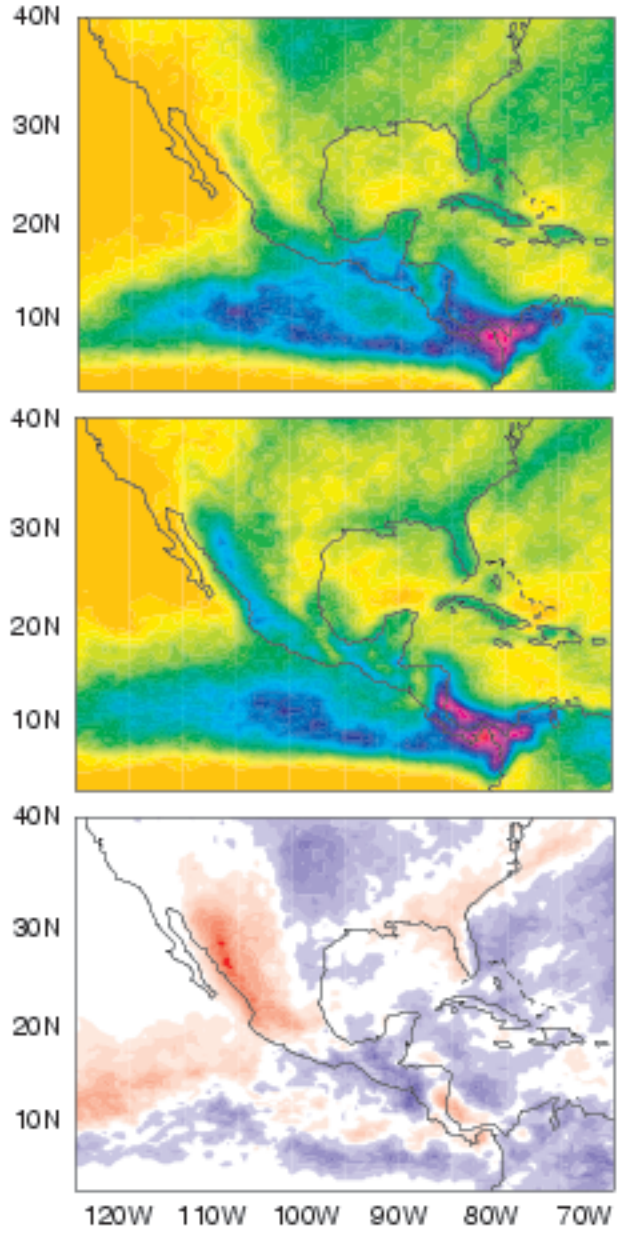

Figure 14. Frequency of occurrence of clouds with tops colder than -38°C as revealed by high-resolution satellite imagery for the years 1990-93. (top) June, (middle) July, (bottom) the difference of July minus June. In most years, the northward shift of the rainfall in northwestern Mexico and Arizona occurs rather abruptly around July 1. Despite this shift, the same distinctive signature of the orography and coastal geometry is evident during both months over much of Central America.

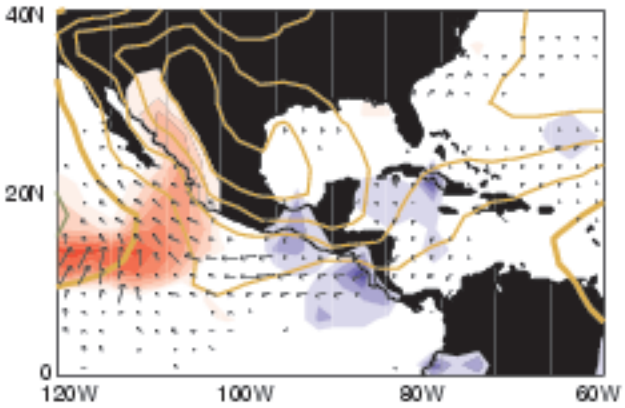

Figure 15. July minus June differences in surface winds (arrows), sea-level pressure (contours: gold denotes pressure increases; zero contour thickened), and rainfall (shading: red denotes increases and blue decreases). The freshening of the trades over much of Central America is related to the rise in sea-level pressure over Mexico. The prevailing northwesterly winds along the west coast of Mexico weaken, allowing surges of moist southerly flow to penetrate into the Gulf of California. The linkage between month-to-month changes in the continental monsoon and the ITCZ appears to be stronger in the microwave sounding unit imagery and rain gauge data shown here than in the infrared imagery shown in the previous figure.

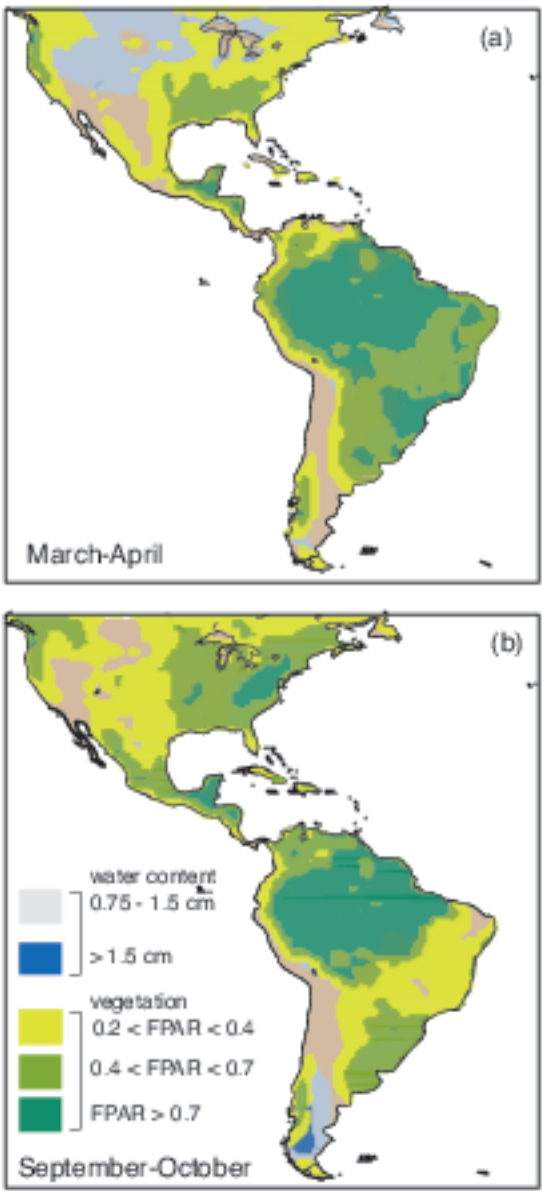

Figure 16. March-April mean (upper panel) and September - October mean (lower panel) soil moisture and vegetation (FPAR). Soil moisture and FPAR as in Fig. 7.

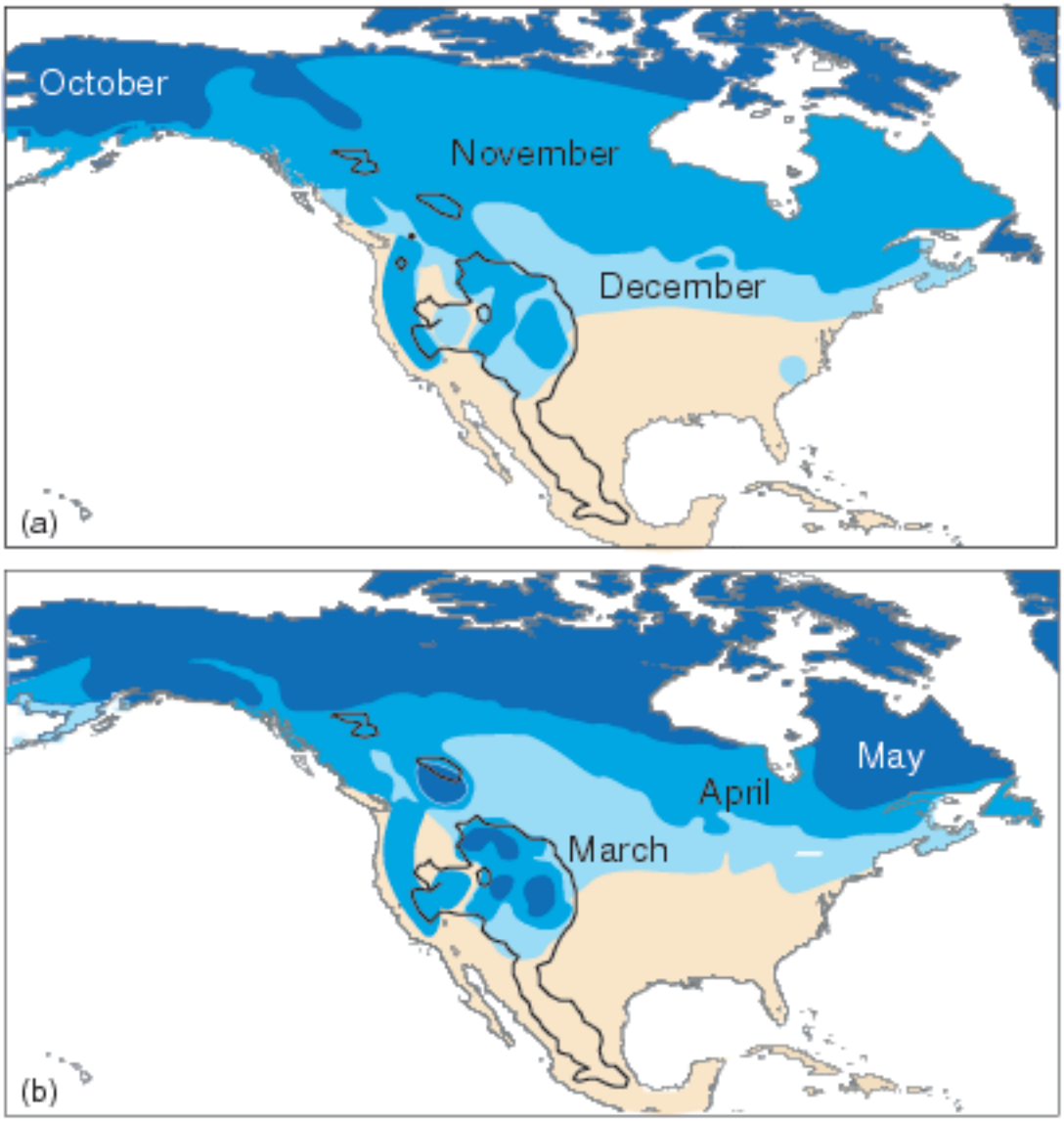

Figure 17. Seasonal march of the snow line at (a) the beginning and (b) end of Northern Hemisphere winter. Darker blues indicate cooler temperatures. Elevation contour is 1500 m.

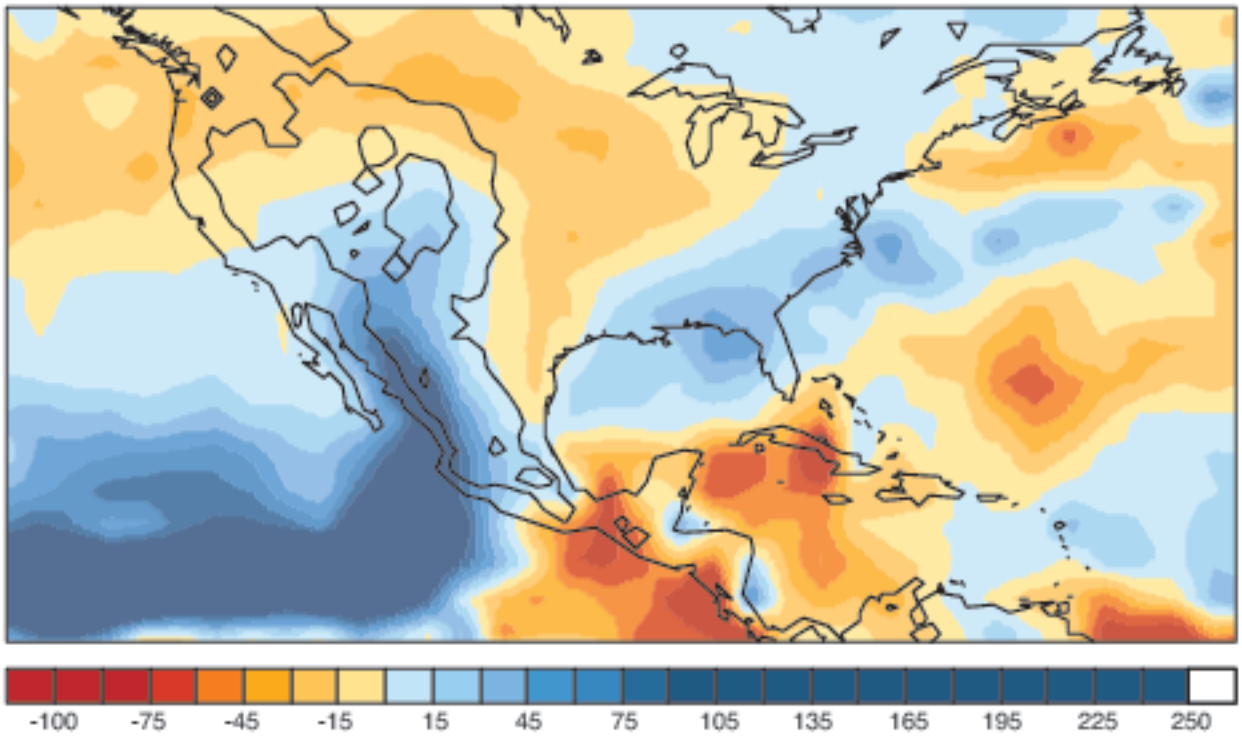

Figure 18. Climatological mean July minus June precipitation (mm/month).

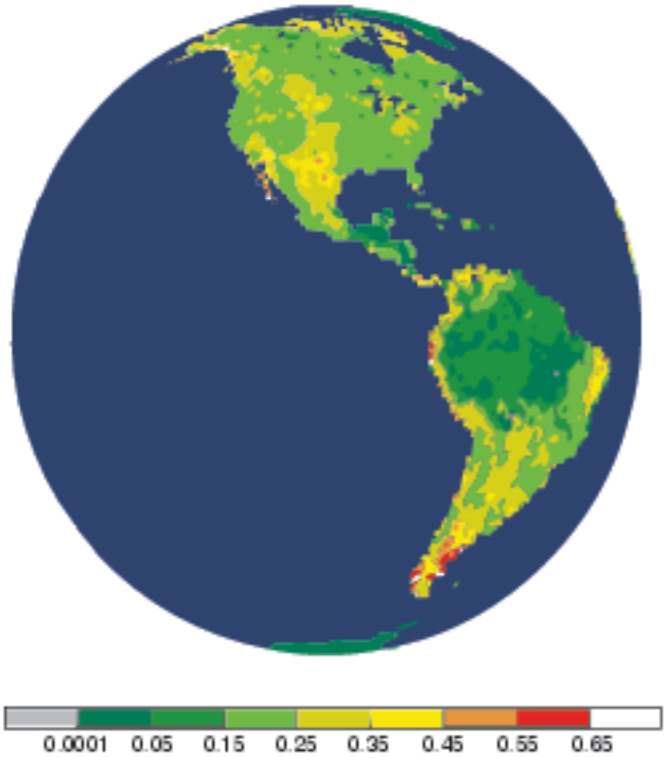

Figure 19. Interannual variability of leaf area index (LAI). The index is the ratio of the one-half of the leaf area to the area of the ground surface.

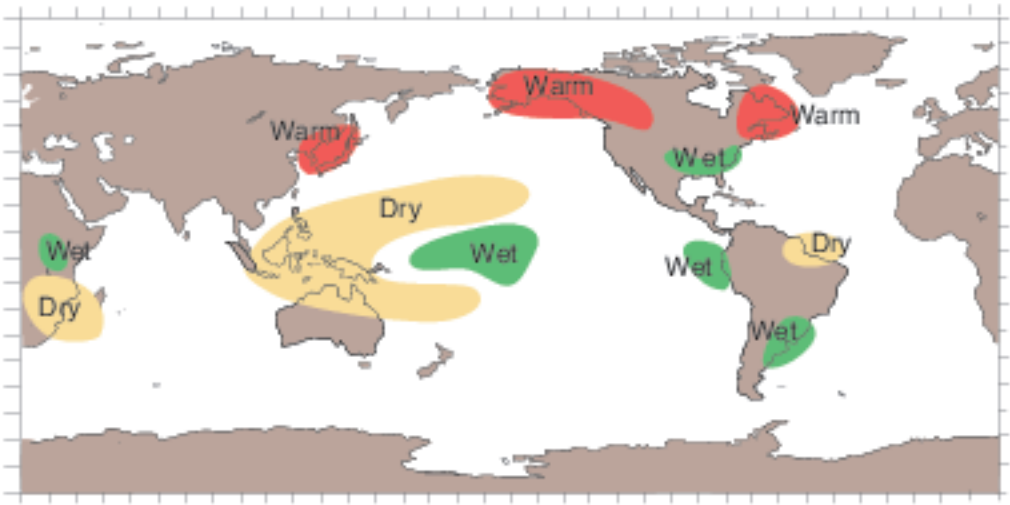

Figure 20. Summary of the major large-scale climate anomalies associated with the warm phase of the ENSO cycle during the Northern Hemisphere winter.

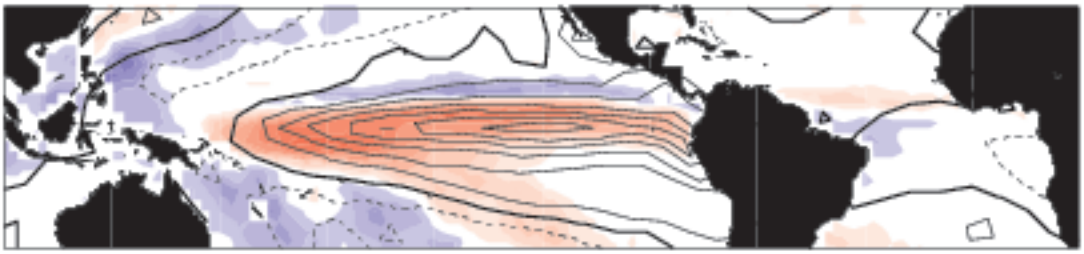

Figure 21. Sea surface temperature anomalies (contour interval 0.2°C) and ocean rainfall anomalies during a typical warm episode of the ENSO cycle. Enhanced rainfall, indicated by the red shading, is observed over the region of above-normal sea surface temperature, and reduced rainfall, indicated by the blue shading, is observed throughout much of the surrounding region and over the tropical Atlantic adjacent to Northeast Brazil.

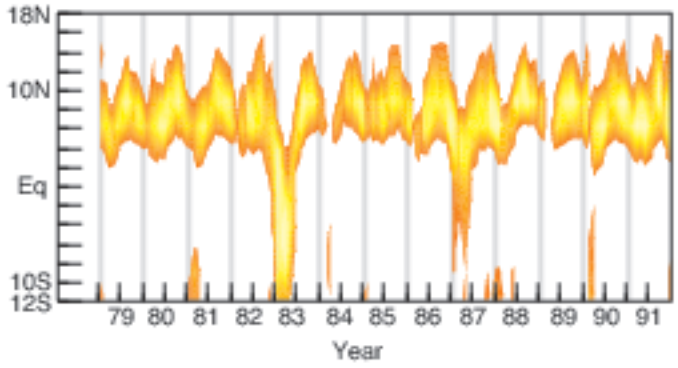

Figure 22. Time-latitude sections of the core of the heavy rainfall associated with the Pacific ITCZ, averaged over longitudes 180-110°W. Estimated rainfall amounts range from 20 cm per month for the orange up to ~50 cm per month for the yellow. Each year the ITCZ is closest to the equator from February through April. The rainy seasons of 1983 and 1987 fell within warm episodes of the ENSO cycle.

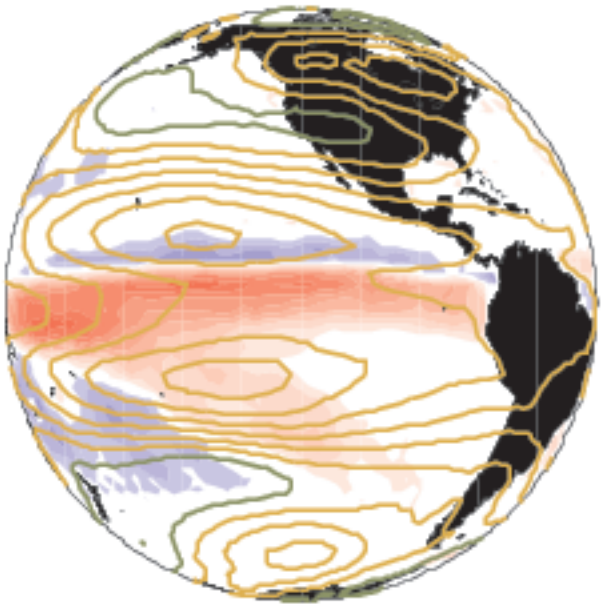

Figure 23. Anomalous rainfall observed during a typical warm episode of the ENSO cycle (colored shading, repeated from Fig. 21) shown with the corresponding pattern of anomalies in mean tropospheric temperature (contours: gold positive and green negative). The pair of temperature extrema straddling the equator in the eastern Pacific are warm anomalies, which correspond to anomalous anticyclonic gyres in the upper-tropospheric flow. These disturbances in the upper-level flow are responsible for the wide-ranging impacts of ENSO upon the climate of the Americas.

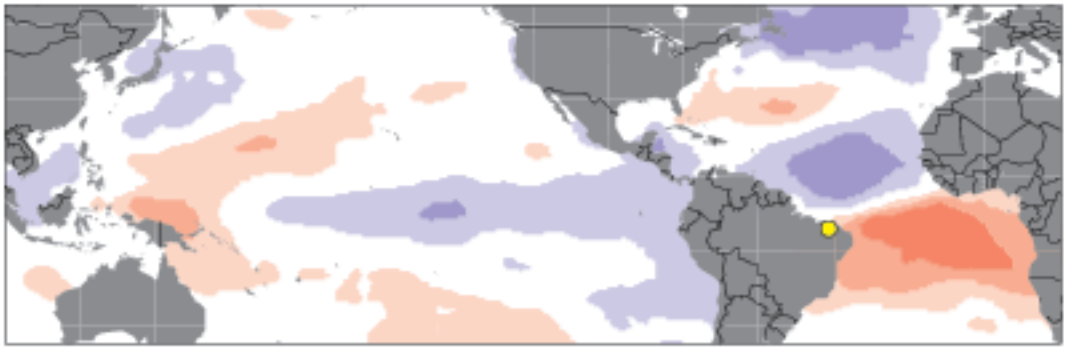

Figure 24. Correlation between average February through May precipitation in northeast Brazil (yellow dot) and sea surface temperature. Red (blue) shading indicates regions in which above-normal sea surface temperatures tend to be observed in conjunction with the above (below) normal rainfall in northeast Brazil. The strongest correlations are on the order of 0.7. Northeast Brazil rainfall tends to be more strongly correlated with Atlantic sea surface temperatures than with Pacific sea surface temperatures.

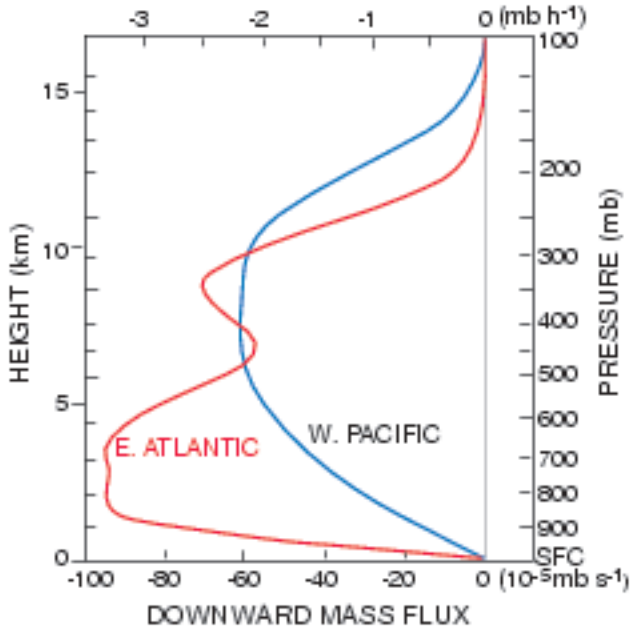

Figure 25. Contrasting vertical mass flux profiles in disturbed regions of the ITCZ in the eastern Atlantic and the "warm core" region of the western Pacific. In the ITCZ the low-level convergence (indicated by the large negative vertical derivative) is concentrated within the lowest 1.5 km, whereas in the western Pacific it is much weaker and extends all the way up to 5 km.

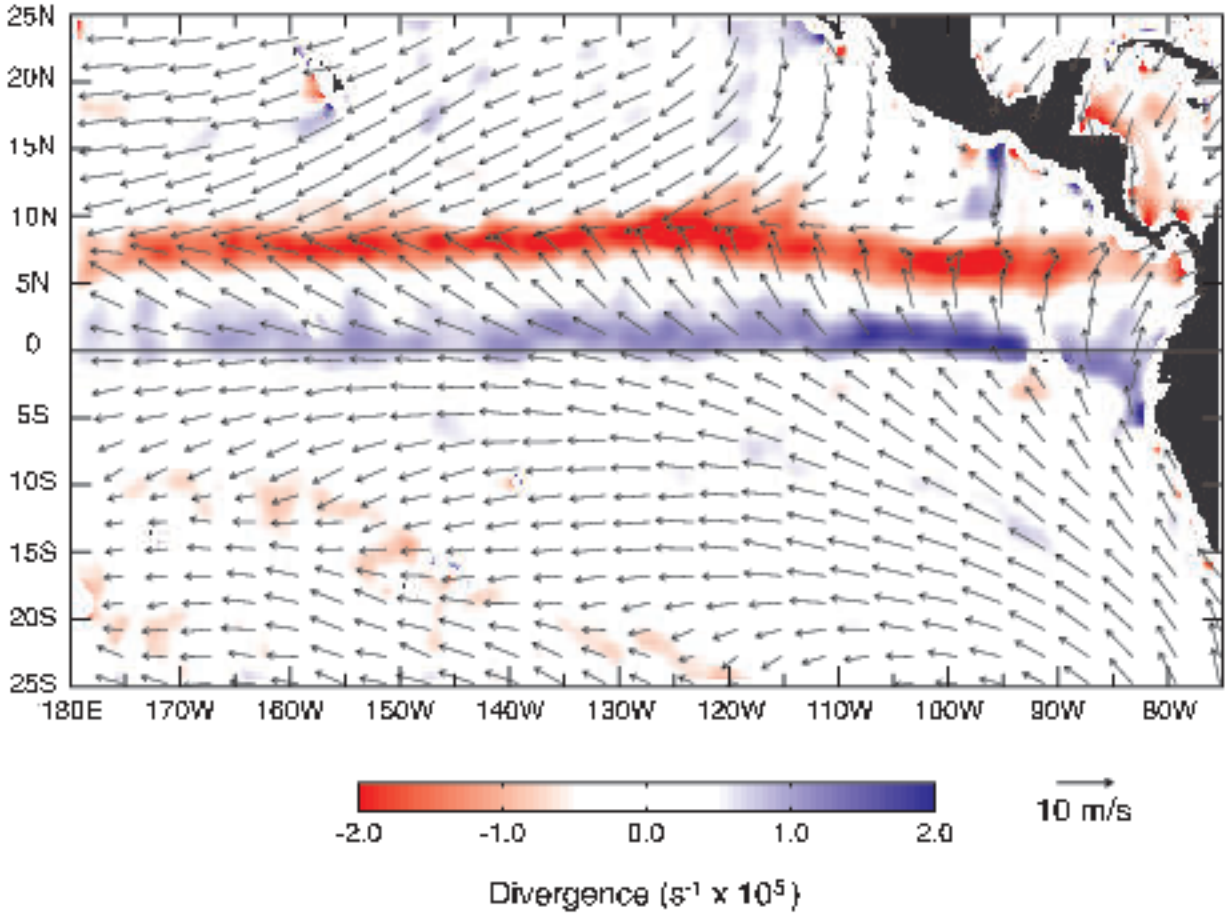

Figure 26. NASA QuikSCAT scatterometer 10-m vector wind averaged for November 1999 (vectors) and the corresponding divergence field. Red and blue denote convergence and divergence, respectively. Shading units in increments of 10^{-5} s^{-1}.

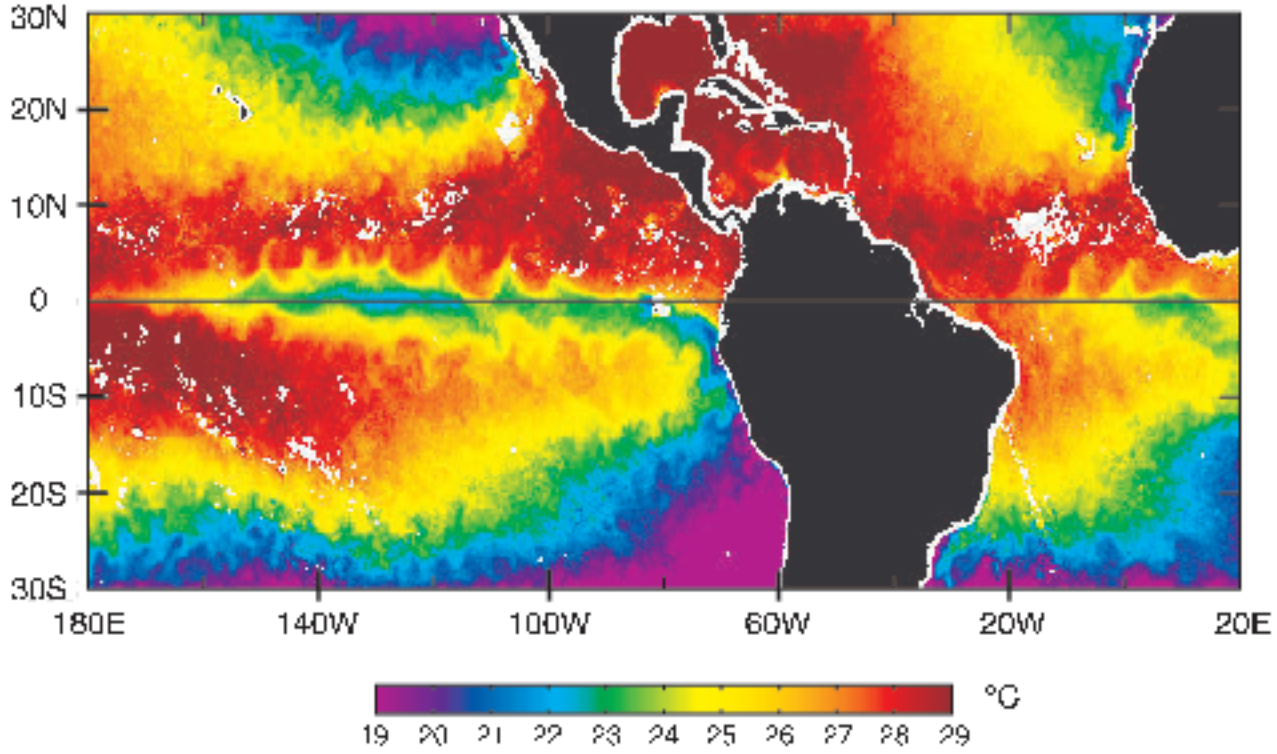

Figure 27. Three-day composite average maps of sea surface temperature for 11-13 July 1998, during a time of year when the equatorial Pacific and Atlantic are typically cool. The maps are based on measurements from a satellite microwave radiometer (TMI). White areas represent land or rain contamination. The sharp northern edge of the cold tongue is distorted by westward-propagating tropical instability waves which originate in the ocean, but produce a distinct signature in the fields of cloudiness and wind speed.

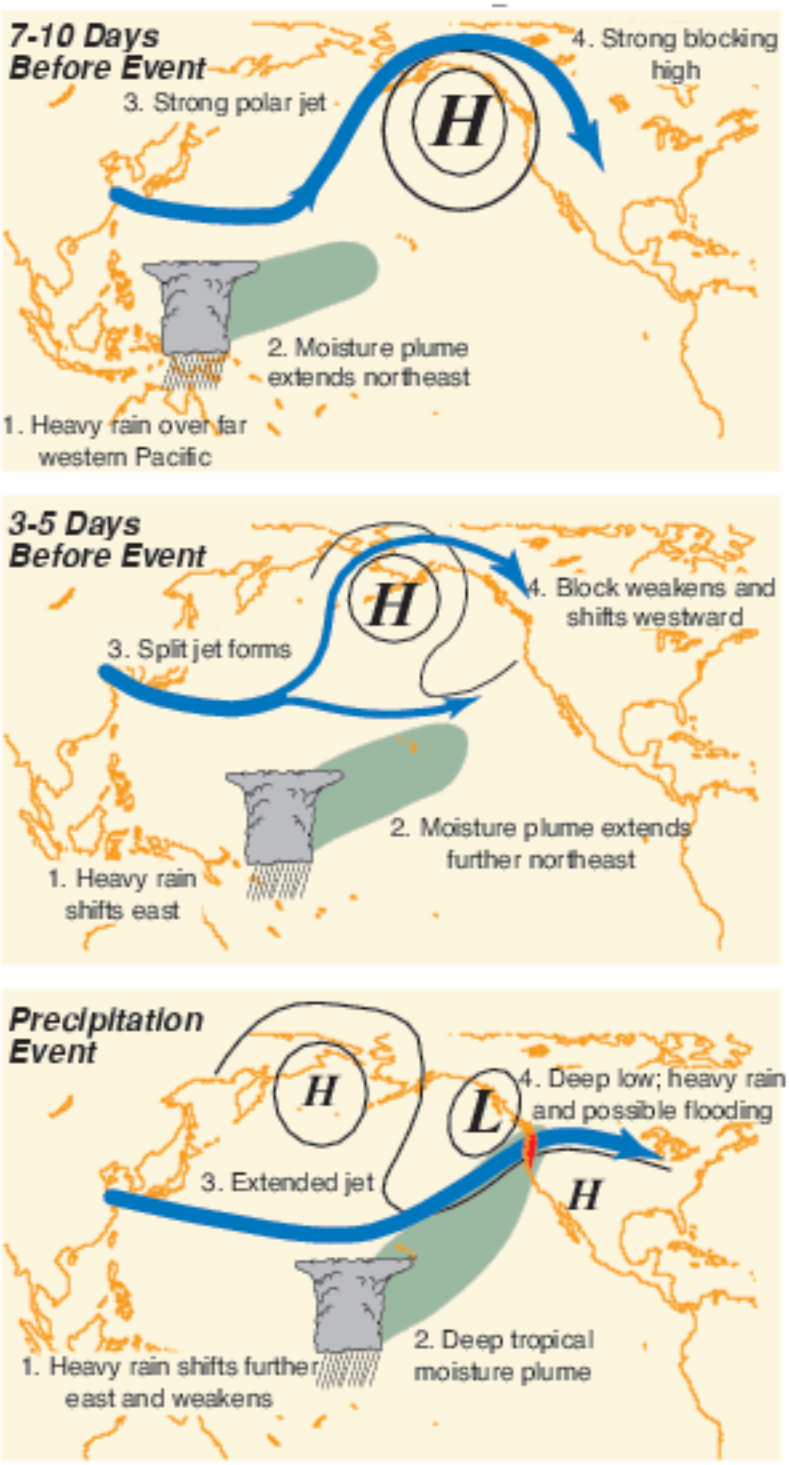

Figure 28. Typical wintertime weather anomalies preceding heavy precipitation events over the northwestern U.S.

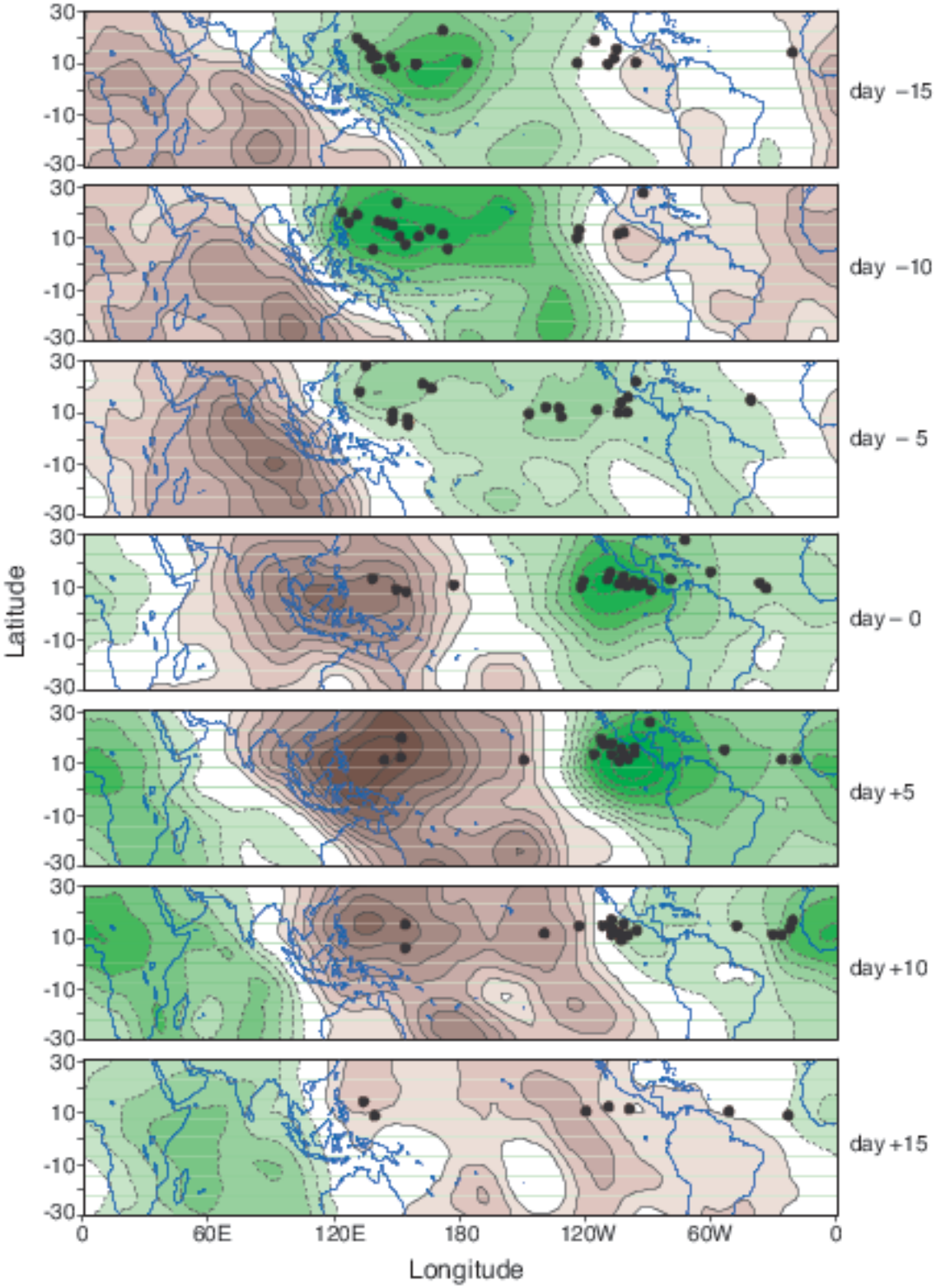

Figure 29. Composited evolution of 200 hPa velocity potential anomalies (10^6 m^2 s^{-1}) and points of origin of weather systems that developed into hurricanes or typhoons (●).

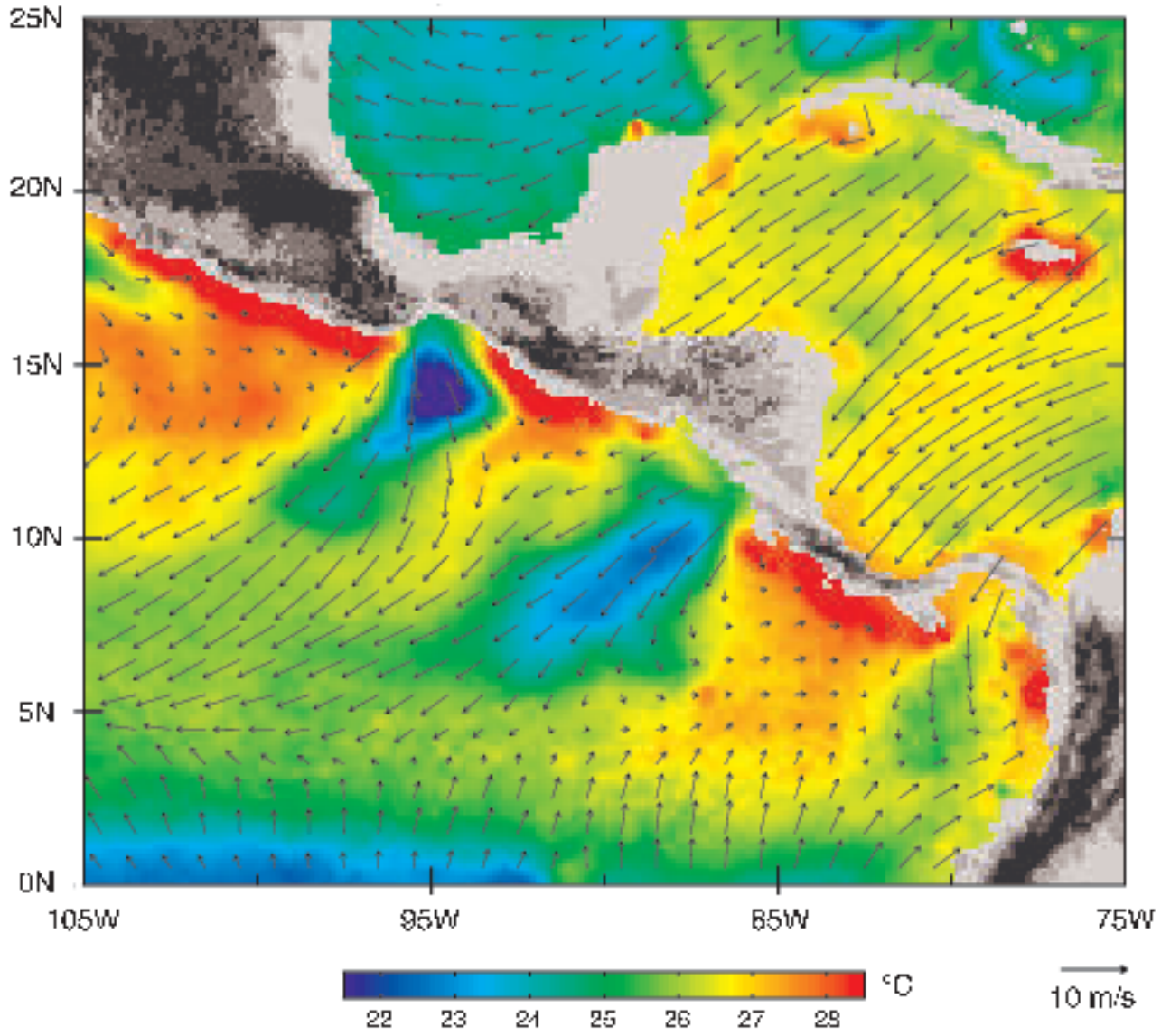

Figure 30. Satellite measurements of surface wind and sea surface temperature averaged for January 2000. Dark shading over land indicates elevation in excess of 300 m. Strong offshore flow downstream of the gaps in the mountain ranges, with monthly mean wind speeds as high as 10 m s^{-1}, gives rise to local sea surface temperature minima, indicated by the lighter red shading in the figure and enhanced chlorophyll concentrations (Fig. 5).

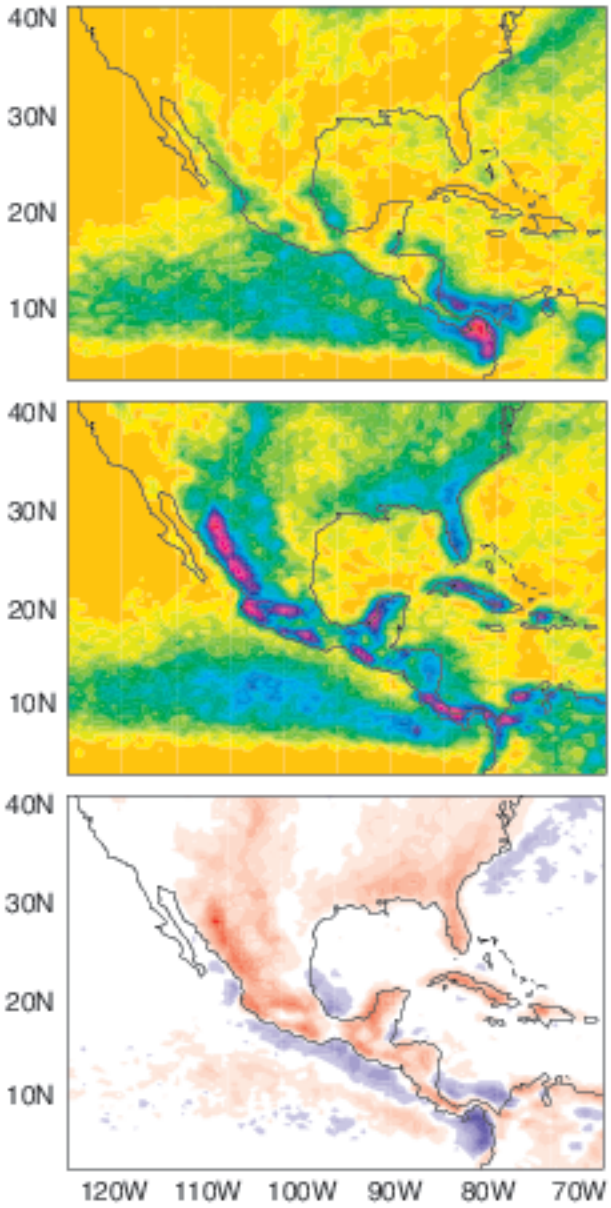

Figure 31. Frequency of deep convection as indicated by the occurrence of clouds with tops colder than -38°C at two different times of day during July. Around 5 AM local time (top) the highlands are cloud free and the offshore waters experience the highest frequency of convective clouds, whereas around 5 PM local time (middle), convection tends to be concentrated over the high terrain and the compensating subsidence tends to keep offshore waters relatively cloud free. The difference between 5 PM minus 5 AM (bottom panel) shows even more clearly the complex influences of the mountain ranges and the shape of the coastline. It is interesting to note how at ~5 PM, the continental monsoon and the ITCZ are well separated, but at ~5 AM they appear to be nearly merged.

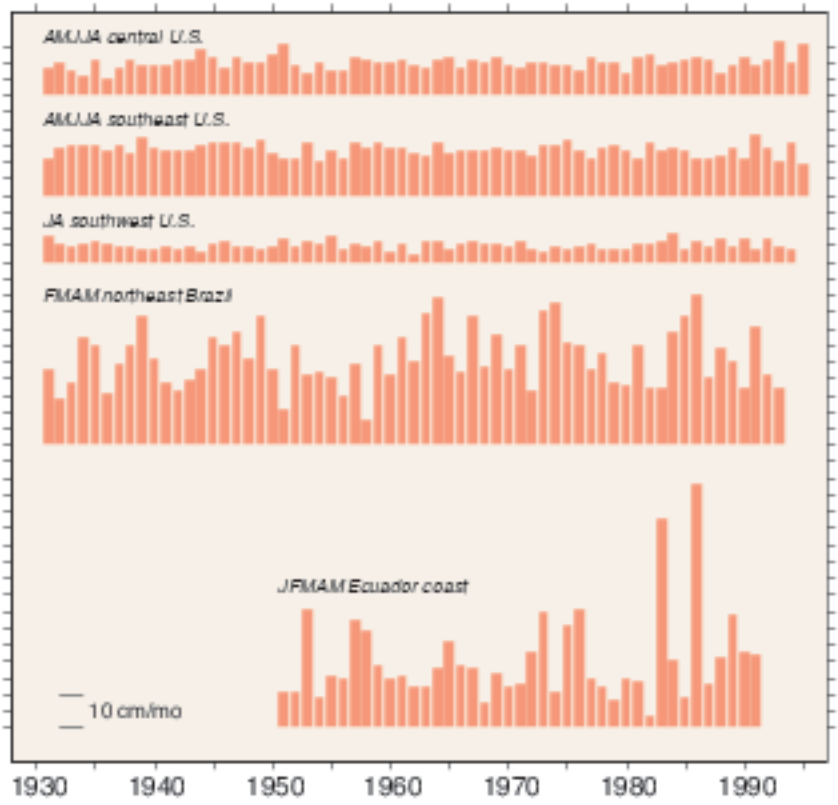

Figure 32. Time series of warm season rainfall over selected regions: U.S. Great Plains; southeast U.S.; Arizona; Ceara, Brazil; and Guayaquil, Ecuador. Average months as indicated.

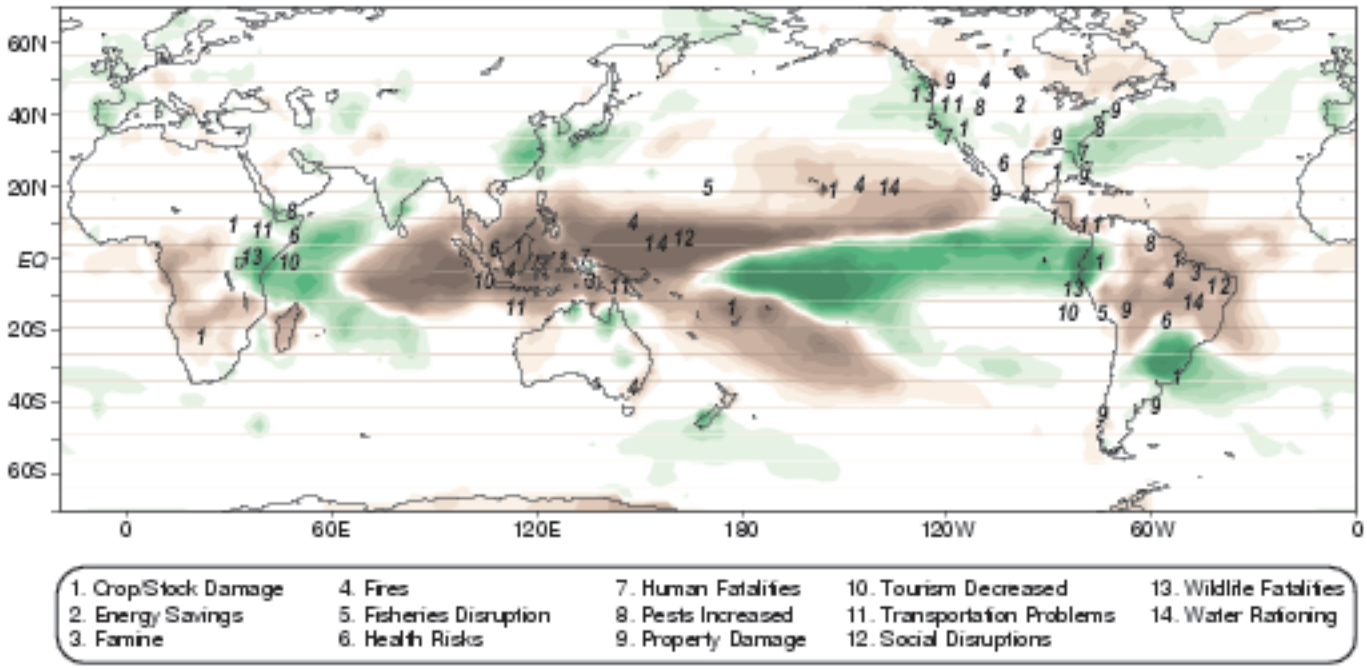

Figure 33. Nature of global El Niño impacts during 1997-1998.

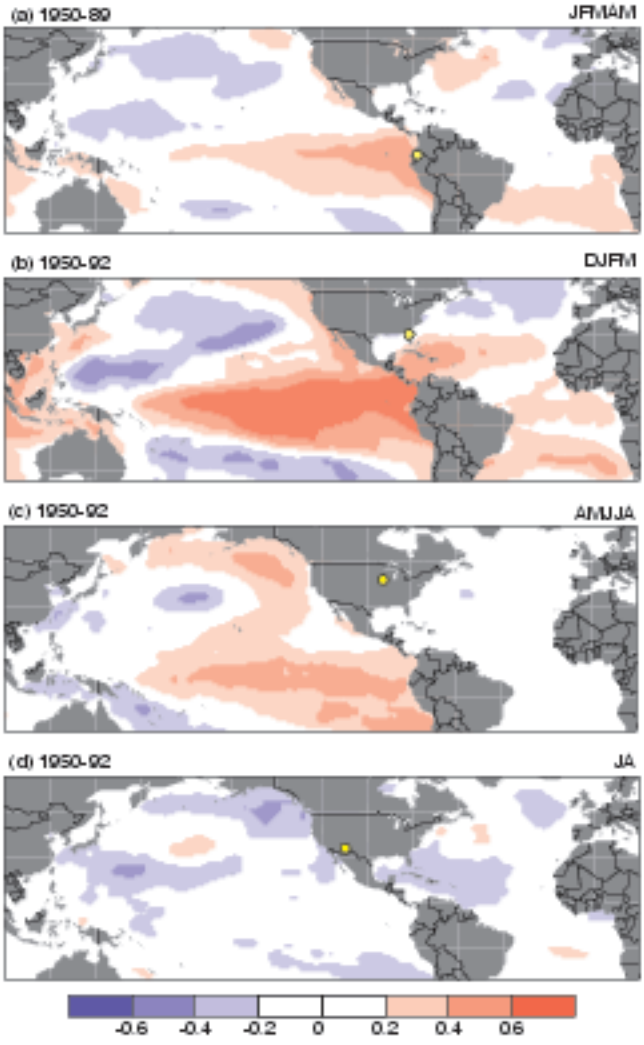

Figure 34. Simultaneous linear correlations between seasonal-mean rainfall in the indicated region (yellow dot) and Pacific and Atlantic sea surface temperature anomalies. Averaging months and periods of record as indicated. See also Fig. 24.

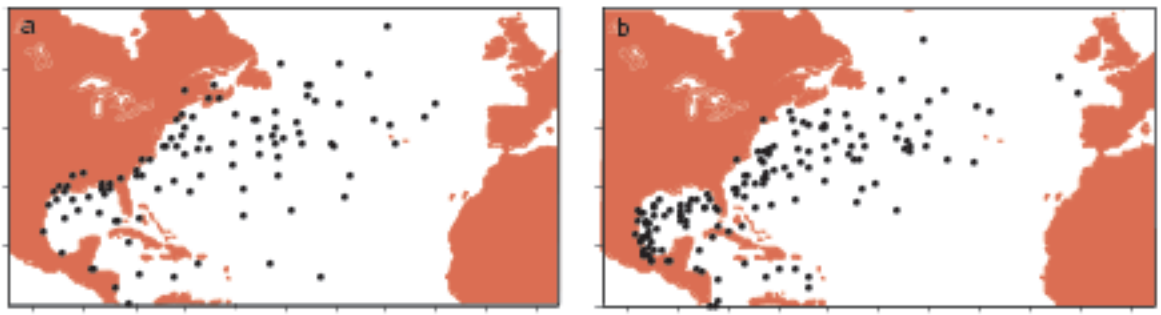

Figure 35. Hurricane positions on the last day that they exhibit hurricane-force winds during the (a) 25 warmest and (b) 25 coldest years in terms of sea surface temperature in the equatorial cold tongue region (6°N-6°S, 180-90°W) based on the period of record 1886-1992.

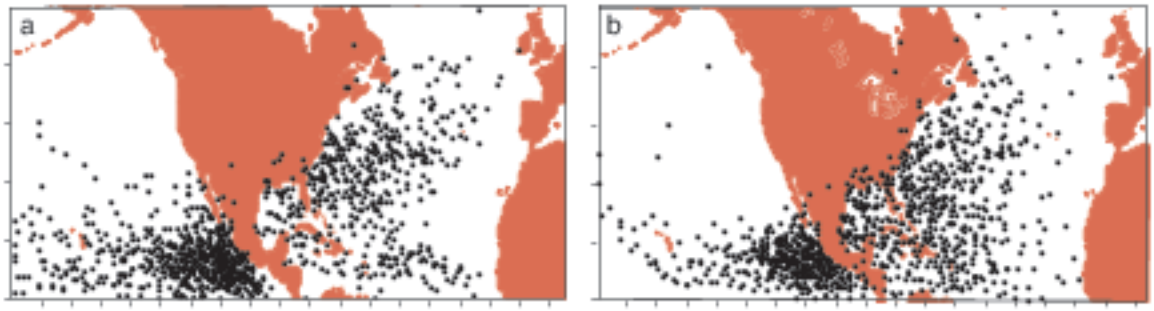

Figure 36. Daily hurricane and tropical cyclone positions during the (a) 10 warmest and (b) 10 coldest years in terms of sea surface temperature in the equatorial cold tongue regions based on the period of record (1949-1992).

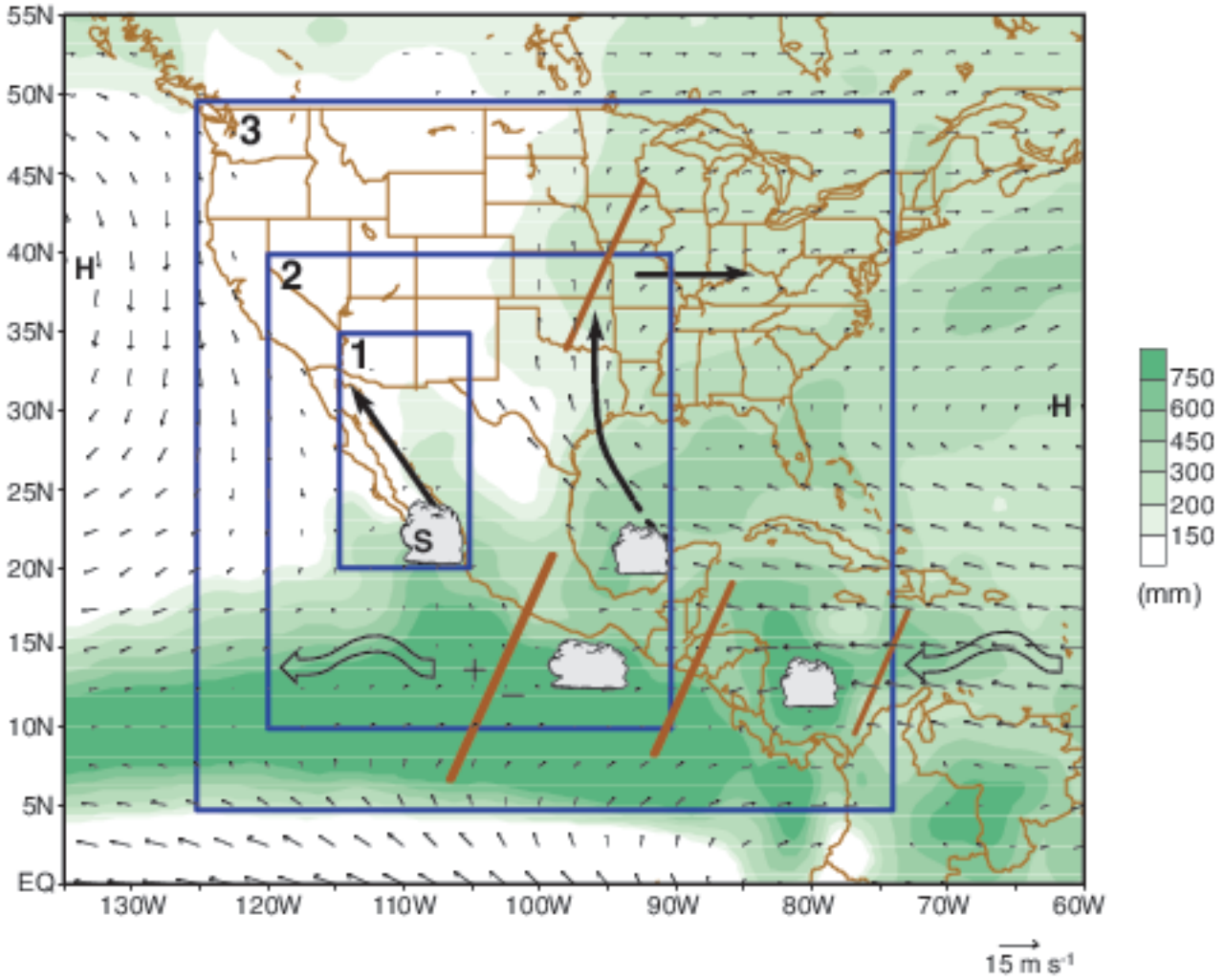

Figure 37. Schematic figure illustrating the implementation plan for the North American Monsoon Experiment (NAME). Analytic, diagnostic, and model development activities will be organized using a multiscale approach. NAME includes specific research objectives addressing mesoscale (Tier 1), regional scale (Tier 2), and continental scale (Tier 3) phenomena. The N-S arrows are the Gulf of California and Great Plains low level jets. Squiggly arrows represent tropical easterly waves (TEW) and angled lines show the intensification of a TEW as it moves westward. The angled line over the Central Plains indicates a midlatitude disturbance that is propogating eastward, as indicated by the arrow. "S" indicates the origin of a Gulf of California moisture surge and the 'H" indicates the locations of subtropical high pressure systems, specifically the Bermuda high in the Atlantic and the eastern Pacific subtropical high.

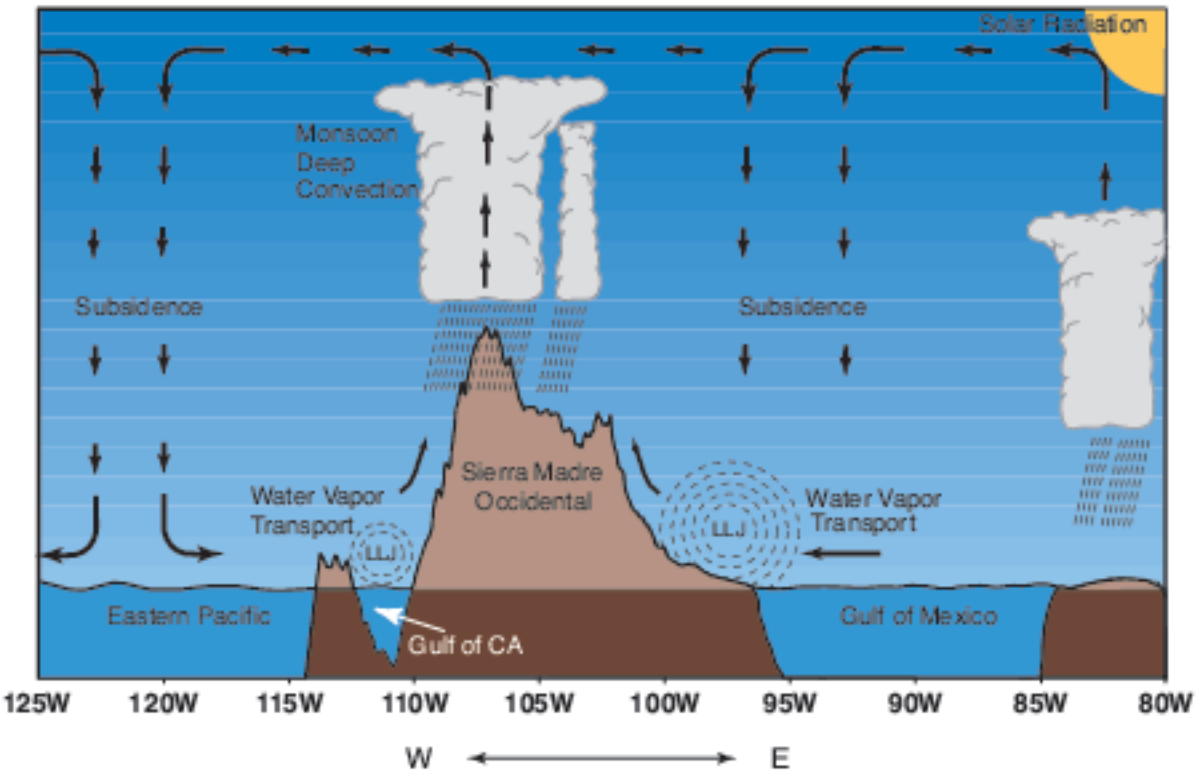

Figure 38. Schematic vertical (longitude-pressure) cross section through the North American monsoon system at 27.5°N illustrating processes and phenomena that contribute to the budgets of heat and water in the core monsoon region.

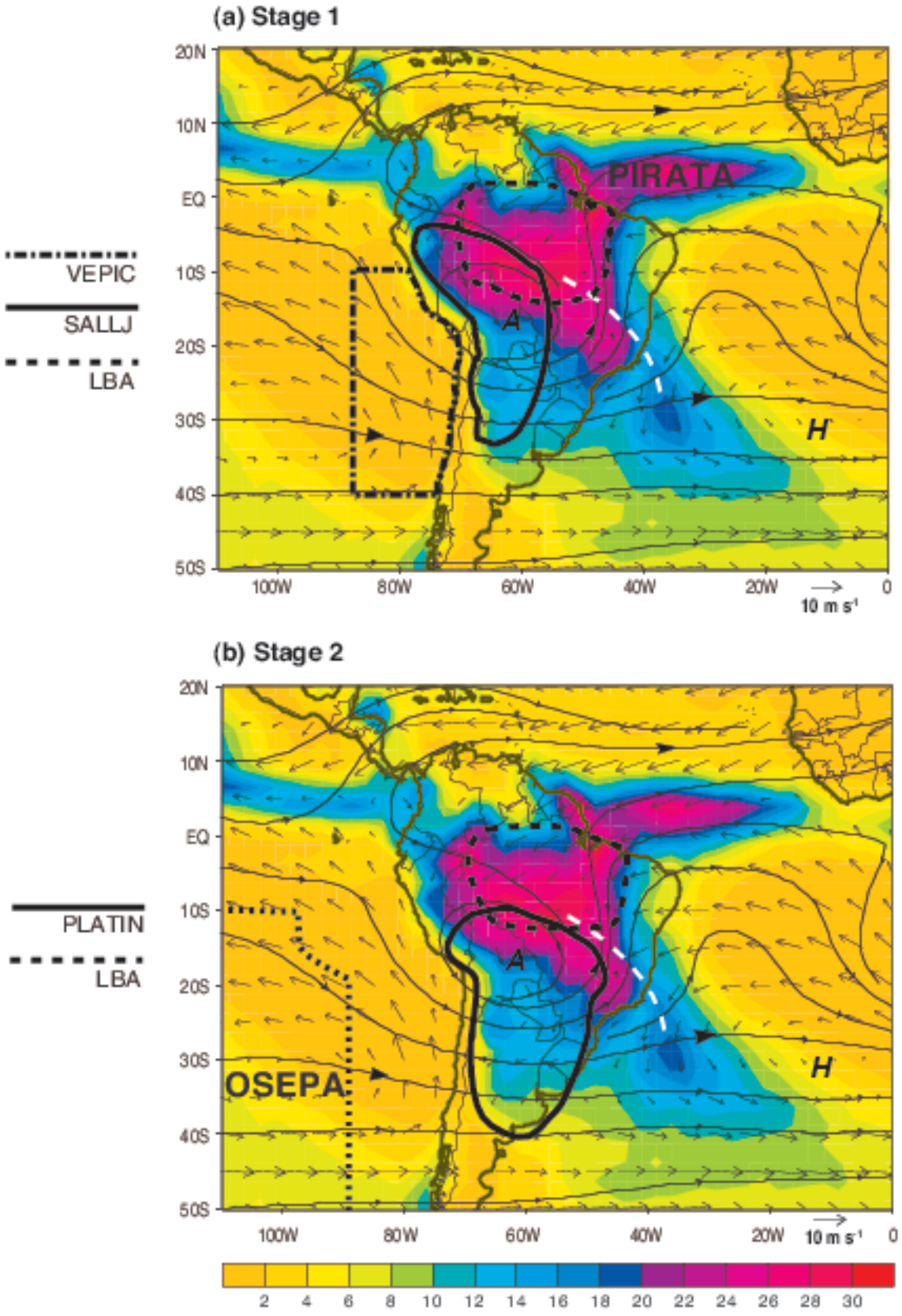

Figure 39. Implementation plan for **MESA** (Monsoon Experiment South America) will have two stages conducted in sequence: (a) Stage 1, a field study leading to better description and understanding of the role of the South American low-level jet (**SALLJ**) in climate variability and **VAMOS EPIC (VEPIC)** studies of ocean-atmosphere-land interactions in the region of the southeastern Pacific Ocean and western South America, and (b) Stage 2, a study of the hydroclimatology of the La Plata River basin. **LBA** (Large-scale Biosphere-Atmosphere in Amazonia) is a GEWEX program focusing on the water and energy budgets of the Amazon River basin. **PIRATA** (Pilot Research Moored Array in the Atlantic) and **OSEPA** (proposed Ocean Southeast Pacific Array) are moored buoy arrays designed for enhanced ocean-atmosphere climate monitoring.

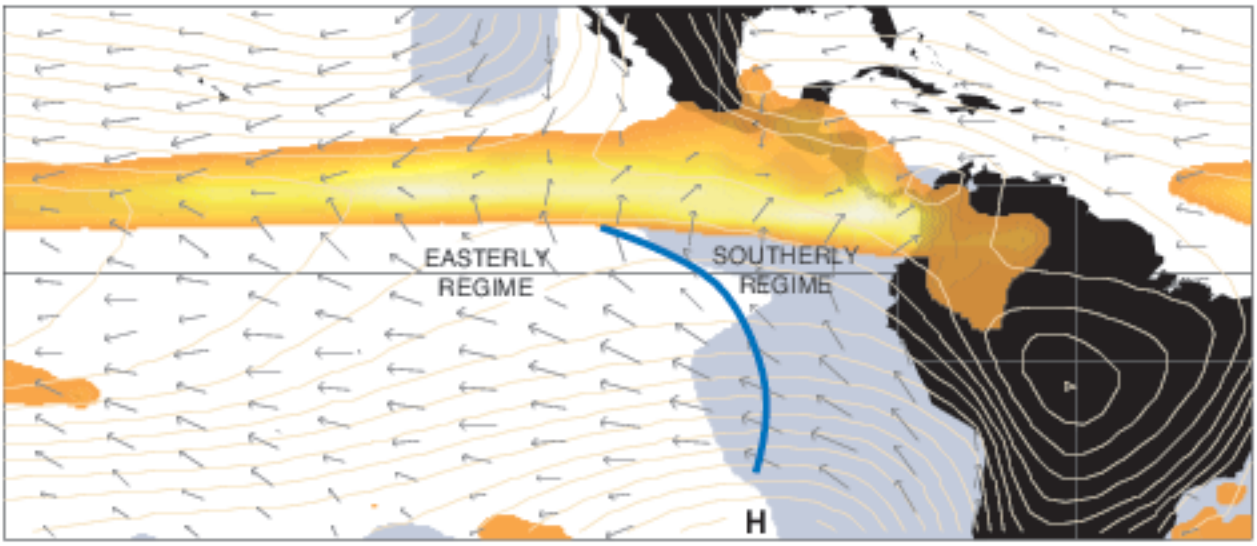

Figure 40. Equatorial wind regimes as defined in the text, superimposed upon the average September-October climatology. Surface vector wind, rainfall, and stratus cloud sources and plotting conventions as in Fig. 2. The contours indicate sea-level pressure (contour interval 1 mb). The heavy line depicts the "ridge line" in the sea-level pressure field, i.e., the highest pressure at each latitude.

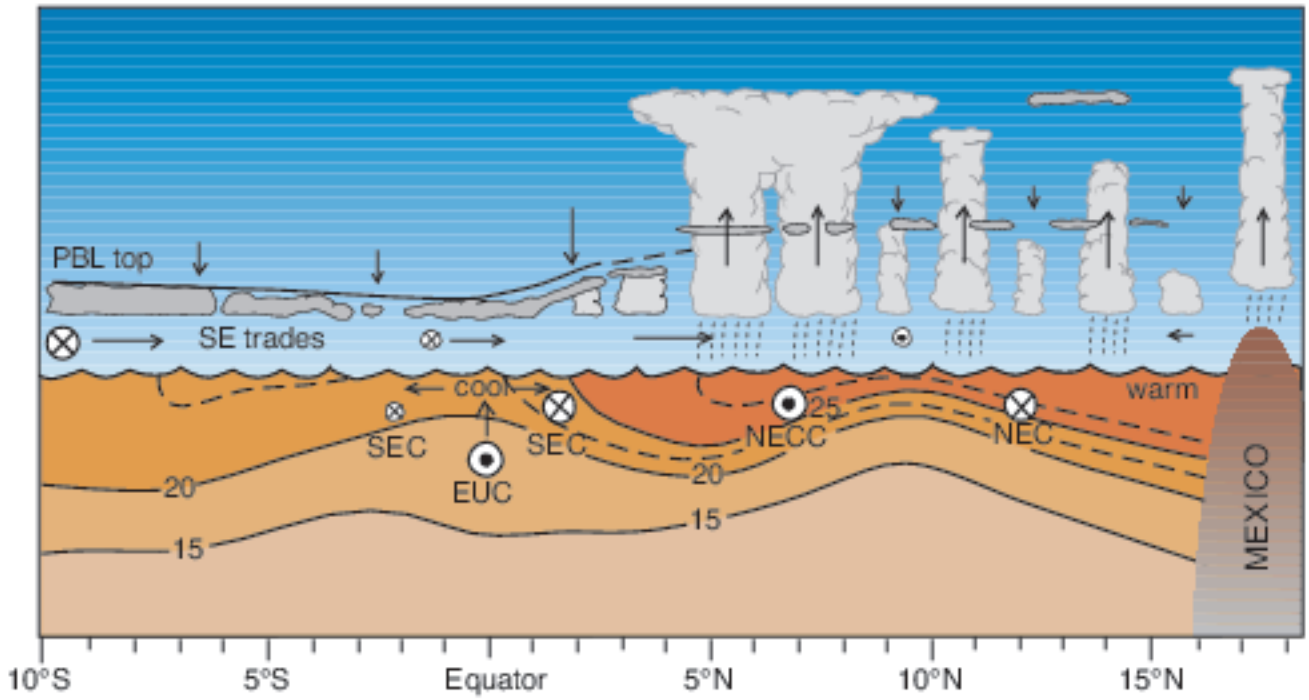

Figure 41. Idealized cross section through the ITCZ/cold tongue complex in the monsoonal regime showing the atmospheric meridional circulation, atmospheric boundary layer depth, and the oceanic thermal structure. SEC refers to the South Equatorial Current, NECC to the North Equatorial Countercurrent, and EUC to the Equatorial Undercurrent. The heavy cloud denotes the position of the ITCZ. Encircled x's (dots) denote westward (eastward) flowing winds or currents.

Figure 42. PACS SONET upper-air stations for enhanced climate monitoring.

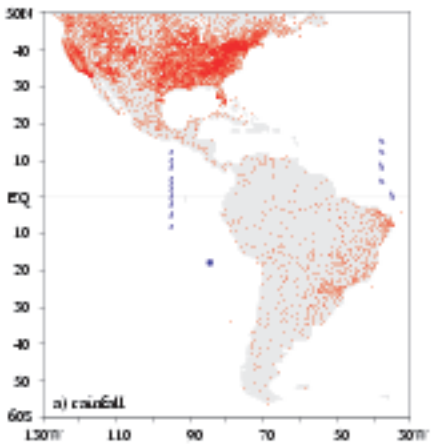

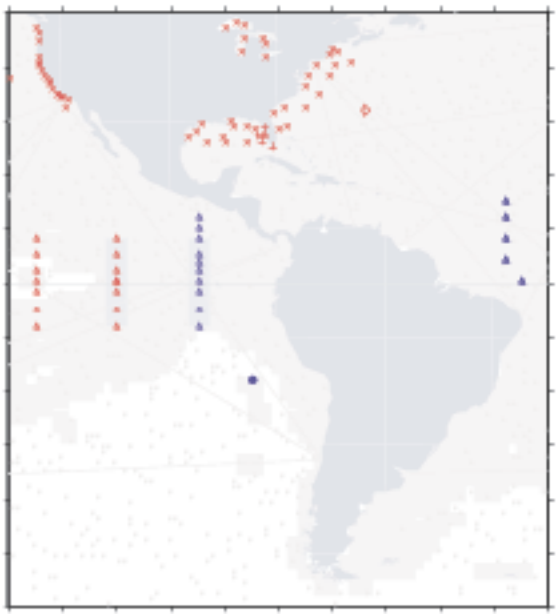

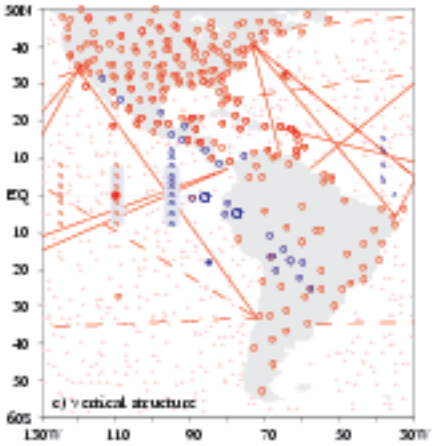

daily rain gauges (dots)

TRMM/ATLAS (not shown)

satellite estimates (not shown)

CLIVAR enhanced monitoring activities are in blue:

enhanced ATLAS (triangles)

IMET (dot)

Raobs (circles)

ATLAS (triangles)

current meter (dot)

Ocean Station S (diamond)

satellite estimates (not shown)

ARGO (dots over oceans)

VOS (solid and dashed lines)

CLIVAR enhanced monitoring activities are indicated in blue:

SONET (circles)

enhanced ATLAS (triangles)

acoustic thermometry profiler (G)

TAO tender enhanced monitoring (shaded rectangles)

IMET (dot)

Figure 43. Existing and proposed elements of the climate observing system that are of importance to US CLIVAR Pan American research. Shown schematically are (a) existing rainfall observing stations, (b) locations of existing and proposed ocean surface temperature measurements, and (c) existing or proposed locations for vertical profile observations of the atmospheric and oceanic state. Red symbols indicate operational and quasi-operational observations; blue symbols indicate US CLIVAR-enhanced climate monitoring observations.